High-field Shubnikov–de Haas oscillations in the topological insulator Bi_{2}Te_{2}Se

Jun Xiong, Yongkang Luo, YueHaw Khoo, Shuang Jia, R. J. Cava, and N. P. Ong

Phys. Rev. B **86**, 045314 — Published 17 July 2012

DOI: 10.1103/PhysRevB.86.045314

High-Field Shubnikov-de Haas Oscillations in the Topological Insulator Bi_2Te_2Se.

Jun Xiong[1], Yongkang Luo[1,*], YueHaw Khoo[1], Shuang Jia[2], R. J. Cava[2] and N. P. Ong[1]
Departments of Physics[1] *and Chemistry*[2]*, Princeton University, Princeton, NJ 08544*
(Dated: June 22, 2012)

We report measurements of the surface Shubnikov de Haas oscillations (SdH) on crystals of the topological insulator Bi_2Te_2Se. In crystals with large bulk resistivity (∼4 Ωcm at 4 K), we observe ∼15 surface SdH oscillations (to the $n = 1$ Landau Level) in magnetic fields B up to 45 Tesla. Extrapolating to the limit $1/B \to 0$, we confirm the $\frac{1}{2}$-shift expected from a Dirac spectrum. The results are consistent with a very small surface Lande g-factor.

PACS numbers: 72.15.Rn,73.25.+i,71.70.Ej,03.65.Vf

I. INTRODUCTION

In Topological Insulators, the surface electrons occupy helical Dirac states in which the spin is locked perpendicular to the momentum[1–4]. In three-dimensional examples, the topological surface state was observed by angle-resolved photoemission spectroscopy (ARPES)[5–8]. Scanning tunneling microscopy (STM) has also been applied extensively[9–11]. In transport experiments, quantum oscillations of the surface electrons have been observed in Bi_2Te_3[12], and in (Bi,Sb)Se_3[13]. The Quantum Hall Effect was also observed in a thick film of strained HgTe[14]. However, in the Bi-based materials, progress has been slowed by the small surface conductance G^s relative to the bulk term G^b. We report measurements on crystals of Bi_2Te_2Se in which G^s/G^b ∼1 and SdH oscillations with large amplitudes are observed at high fields. By tracking the Landau Level (LL) extrema towards the quantum limit, we observe directly the $\frac{1}{2}$-shift that distinguishes the Dirac spectrum from the Schrödinger case. Our results address the question whether the spin-Zeeman energy affects the LL sequence in the quantum limit.

Landau quantization of the surface Dirac spectrum was previously observed in Bi_2Se_3 by STM[10,11]. Nonetheless, high-B transport experiments to approach the quantum limit are important to search for novel states. In addition, accurate determination of the $\frac{1}{2}$-shift associated with the Berry phase provides the best test for whether the SdH oscillations arise from surface topological states or bulk states (this requires a large B to reach the $n =$ 1 LL).

In a magnetic field $\mathbf{B}$ normal to the surface, the Dirac states are quantized into Landau Levels (LLs). As B is increased, sequential emptying of the LLs leads to oscillations in G^s. We follow the customary practice of defining the "index field" B_n as the field at which the Fermi energy E_F lies between two LLs, i.e. at the minima in G^s (see Sec. II). A plot of the integers n vs. $1/B_n$ gives a nominally straight line with slope equal to the FS cross-section S_F.

Our interest is in the limit $1/B_n \to 0$. In the Schrödinger case, there are n filled LLs below E_F when the field equals B_n (as defined). By contrast, in the Dirac case, we have $n + \frac{1}{2}$ filled LLs between E_F and the Dirac point (at $E = 0$). The important additional $\frac{1}{2}$ arises because the conduction band and the valence band each contributes half of the states that make up the $n = 0$ LL. Hence, as $1/B \to 0$, the plot of $1/B_n$ vs. n intercepts the n-axis at the value $\gamma = -\frac{1}{2}$ for the Dirac case, whereas the intercept $\gamma = 0$ (mod 1) in the Schrödinger case. The $\frac{1}{2}$-shift was experimentally verified for the Dirac spectrum in graphene, and expressed equivalently as a Berry-phase π-shift[15].

II. RESISTIVITY MAXIMA OR MINIMA?

The index field B_n clearly plays the key role in pinning down the -$\frac{1}{2}$ shift in the index plot. Here we wish to discuss the question of determining B_n when surface and bulk carriers co-exist[16]. In the bismuth-based systems (and other 3D topological insulators), the two-dimensional electron gas (2DEG) on the surface is in intimate contact with bulk electrons which conduct a significant fraction of the applied current. By contrast, the entire current is carried by the 2DEG in graphene and GaAs heterostructures. When E_F falls between adjacent LLs in the QHE regime of graphene, both the 2D conductance G_s and resistance R_{xx} attain a deep minimum (this follows from $R_{yx} \gg R_{xx}$).

However, when a large, parallel bulk conduction channel exists (the case here), the observed conductance matrix is the sum

$$G_{ij} = G^s_{ij} + G^b_{ij}, \qquad (1)$$

where G^b_{ij} is the bulk conductance matrix. As the mobility of the bulk carriers μ_b is very low (50 cm^2/Vs), bulk SdH oscillations are not observable even at 45 T. The additivity of the conductances in Eq. 1 implies that the index fields still correspond to minima in G_{xx}. However, because the bulk G^b_{xx} is dominant, the observed resistance now attains maxima at B_n (i.e. $R_{xx} = G_{xx}/[G^2_{xx} + G^2_{xy}] \sim 1/G_{xx}$). We find that it is least confusing to work with G_{ij} because its components are additive. The results reported here provide an experimental verification of this point.

In many experiments, however, the Hall response is not available. One may still use the SdH oscillations in the

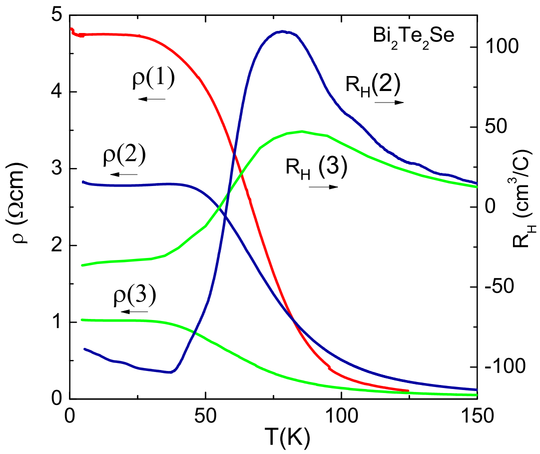

FIG. 1: (color online) A representative set of the observed resistivity ρ and Hall coefficient R_H vs. T in Bi_2Te_2Se (samples identified by the numbers). The magnitudes of ρ and R_H at 4 K vary considerably between annealed samples. In all samples, the carriers are predominantly n-type at 4 K. The change in sign of R_H near 56 K reflects the thermal activation of bulk hole carriers across a gap of 50 mV. The largest SdH amplitudes are observed in samples with $\rho > 4$ Ωcm at 4 K.

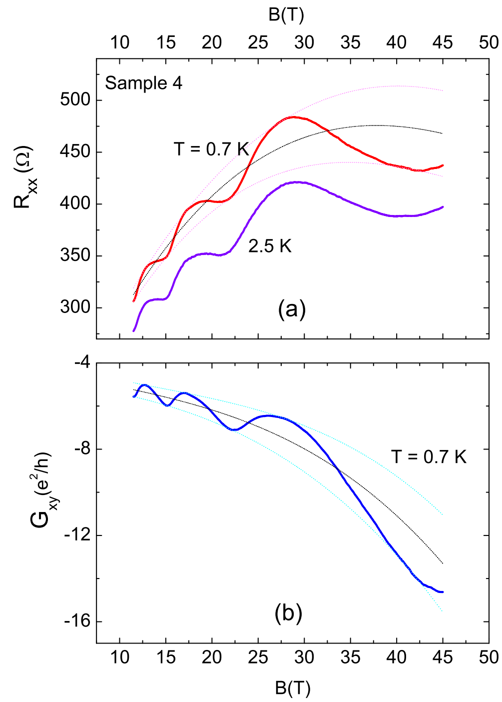

FIG. 2: (color online) The resistance (per square) R_{xx} and Hall conductance G_{xy} in Bi_2Te_2Se (Sample 4). Panel (a) shows the SdH oscillations in R_{xx} vs. B at fields above 11 T at $T = 0.7$ and 2.5 K. At 40 T, the peak-to-peak amplitude is 17 % of the observed resistance. The Hall conductance G_{xy} at 0.7 K is plotted in Panel (b). In both panels, the envelope is the smooth curve passing through the extrema points. The background curve (dashed curve) is determined as the average of the envelope curves.

resistance R_{xx}, provided B_n is identified with its *maxima*. If the wrong choice is made (identifying B_n with minima in R_{xx}), a spurious -$\frac{1}{2}$ intercept will appear for carriers with a Schrödinger dispersion.

A second issue we address is the strength of the Zeeman energy. Strict particle-hole symmetry implies that it is unshifted in energy. On the other hand, a large Zeeman energy $g\mu_B B$ may lead to high-field distortion of the SdH period (g is the surface Lande g-factor and μ_B the Bohr magneton). The in-field STM experiments [10,11] have shown that the $n = 0$ LL is unshifted up to 11 Tesla. This test can be extended to much larger B in transport experiments, but early SdH experiments had limited resolution[12,13]. Values of g as large as 76 have been inferred from low-field SdH oscillations in Bi_2Te_2Se[17].

III. EXPERIMENTAL DETAILS

The large density of Se vacancies (electron donors) in Bi_2Se_3 leads to an n-type semi-metal with a sizeable carrier density ($n_b \sim 10^{18}$ cm^{-3}). By contrast, as-grown crystals of Bi_2Te_3 are p-type because of Te-Bi exchange defects. In the hybrid material Bi_2Te_2Se, the Se ions occupy the innermost layer in each quintuplet layer. This appears to suppress both vacancy formation and Te-Bi exchange defects. Two groups have found that surface SdH oscillations are observed in n-type crystals with greatly reduced n_b[18,19]. Details of the crystal growth for our samples appear in Ref.[20].

Even in carefully annealed crystals, large variations in the values of n_b and the observed resistivity ρ are found[20].

Figure 1 shows traces of ρ vs. T for a representative set (Samples 1, 2 and 3). At 4 K, ρ varies from 1 to 6 Ωcm. Although all these samples exhibit SdH oscillations, the amplitudes are largest when $\rho > 4$ Ωcm at 4 K.

As shown, the Hall coefficient R_H changes from p to n-type as T decreases near 56 K. We have found[21] that the Hall behavior results from the thermal activation of holes into the bulk valence band across a "transport" gap $\Delta_T \sim 50$ mV. Previously, we showed[19] that the surface conductance G^s in Bi_2Te_2Se involves carriers with a high mobility μ_s of 2,800 cm^2/Vs, whereas the residual bulk conductance G^b (from an impurity band) involves n-type carriers with much smaller mobility ($\mu_b \sim 50$ cm^2/Vs). The magnitudes of G^s inferred from k_F and μ_s confirm that the SdH oscillations are from surface states. Ando's group has shown in field-tilt experiments that the SdH period is consistent with surface states[18]. Helical surface states in an isolated Dirac band have been observed by spin-resolved ARPES[22].

The large variation in ρ may be understood by estimating the number defects. If we assume that each de-

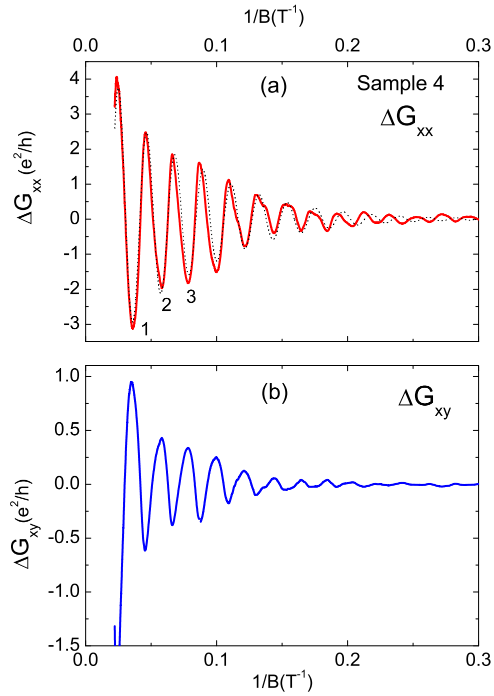

FIG. 3: (color online) The oscillatory component of the conductance ΔG_{xx} (Panel a) and the Hall conductance ΔG_{xy} (Panel b) in Sample 4 plotted against $1/B$ (T = 0.7 K). The two quantities are normalized to e^2/h. The fit of the oscillations (see Fig. 6) yields a surface mobility of 3,200±300 cm^2/Vs, with $k_F\ell = 30$. In Sample 4, G^s accounts for $\sim$ 19% of the total conductance at 4 K. Note the phase shift at low B. The LL indices n = 1,2,3 are indicated for the minima of ΔG_{xx}.

fect (either Se vacancies or Te-Bi exchanges) contributes a carrier, the observed n_b (3×10^{16} cm^{-3} in Samples 1 and 2) corresponds to a defect density of a few parts in 10^{5}[20]. This stringent constraint implies that fluctuations at this level lead to pronounced variations in n_b and ρ. Even in optimally annealed crystals, separate portions of an exposed surface can display different ρ-T profiles. In addition, aging of the surface results in a gradual decrease in the amplitude of the surface quantum oscillations with time (roughly by a factor of 2 over a few weeks for crystals sealed in Ar atmostphere and stored in dry ice). These factors are problematical for high-field transport experiments.

To improve the odds, we cleaved crystals ∼30 minutes before loading the high-field cryostat. Each crystal was contacted by 3 pairs of leads so that both the resistance tensor R_{ij} can be measured over distinct segments. Because the 45-Tesla field cannot be reversed, we employed the reciprocity technique of Ref.[23] to extract both R_{xx} and R_{yx}.

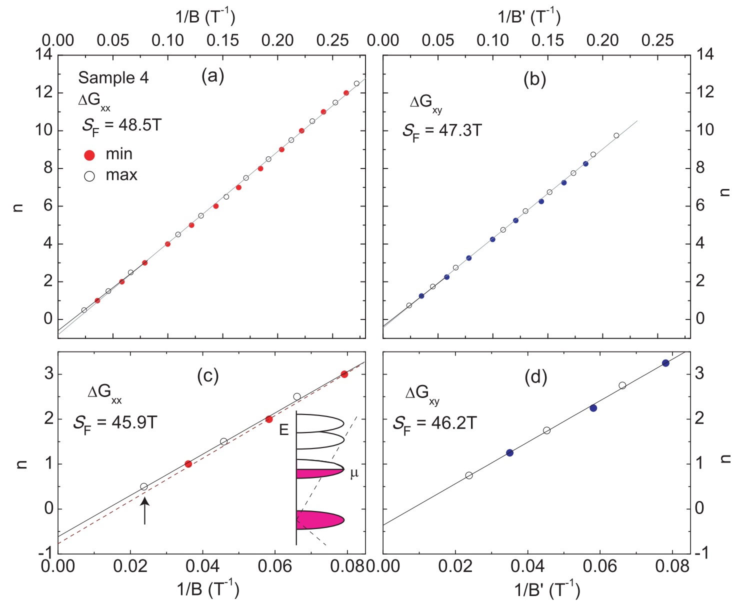

FIG. 4: (color online) The index plots of $1/B_n$ vs. the integers n in Sample 4. In Panel (a), B_n is obtained from the minima of ΔG_{xx}. In Panel (b), the index field B'_n is inferred from the minima of $-\Delta G_{xy}$. B'_n is plotted against $n + \frac{1}{4}$, where the $\frac{1}{4}$ shift arises because the minima in $d\Delta G_{xy}/dB$ align with the minima in ΔG_{xx}. We expand the scale in Panels (c) and (d) to show the intercepts more clearly. In Panel (c), the solid straight line is the best fit to the extrema fields for $n \leq$3. The dashed line is the best fit to all the extrema field shown in Panel (a). The sketch shows E_F in relation to the filled LLs (solid color) in the Dirac spectrum when B = 42.0 T (arrow).

IV. QUANTUM OSCILLATIONS

We report measurements to fields of 45 T in Samples 1 and 4 (in which R_H = -137 and -52 cm^3/C, respectively, at 4 K). The large, well-resolved SdH oscillations in these samples provide an opportunity to investigate the specific issues in the quantum limit. As shown in Fig. 2a, the peak-to-peak SdH amplitude in the resistance R_{xx} in Sample 4 grows with B until it accounts for ∼17% of the total resistance. Because conductances are additive, it is expedient to convert R_{ij} to the conductance $G_{xx} = R_{xx}/[R^2_{xx} + R^2_{yx}]$ and the Hall conductance $G_{xy} = R_{yx}/[R^2_{xx} + R^2_{yx}]$. G_{xy} is plotted in Fig. 2b. Using the envelope of the oscillations (faint curves), we locate the midpoint between adjacent extrema to define the background.

After removing the background, we isolate the oscillatory components ΔG_{xx} and ΔG_{xy} which we plot versus $1/B$ in Fig. 3. The conductance ΔG_{xx} and Hall conductance ΔG_{xy} are plotted in Panels (a) and (b), respectively (both normalized to the quantum of conductance e^2/h). The fit of the oscillations (see Sec. V) yields a surface mobility of 3,200 cm^2/Vs and a metallicity parameter $k_F\ell = 30$. The interesting phase shift apparent at low B is discussed later.

Figure 4a plots the minima of ΔG_{xx} versus n (solid circles). In addition, the maxima of ΔG_{xx} have been plotted as open circles (shifted by $\frac{1}{2}$). The best-fit straight line gives a Fermi cross-section area S_F of 48.5 T. A similar plot based on the extrema of the Hall conductance ΔG_{xy} is shown in Fig. 4b. The minima in $-\Delta G_{xy}$ correspond to $n+\frac{1}{4}$, since the derivative $-d\Delta G_{xy}/dB$ has minima at n. The value of S_F found from ΔG_{xy} (47.3 T) is consistent with the previous value within our resolution. The values of n = 1,2,3 at the minima of ΔG_{xx} are noted in Fig. 3a.

In order to fix the intercept γ, we expand the scale in Fig. 4c. The best-fit straight line passing through the six extrema of ΔG_{xx} intercepts the n-axis at the value γ = -0.61±0.03. Similarly, the high-field extrema of ΔG_{xy} are plotted in Fig. 4d. The intercept for the best-fit line occurs at γ = -0.37±0.03. Within our uncertainties, these intercepts are significantly closer to the ideal value $\gamma = -\frac{1}{2}$ than 0 or 1. Hence, the high-field results provide transport evidence for a Dirac spectrum for the surface states.

Although we do not observe quantized Hall steps in Fig. 3b (the oscillatory component rides on a large tilted background contribution from the bulk Hall current), it is interesting that the peak-to-peak amplitude swing of ΔG_{xy} is ∼0.8 e^2/h per surface for $n = 1$, which is of the order of the quantized Hall conductance value.

In Sample 1, the amplitudes of the observed SdH oscillations are considerably weaker (Fig. 5a). The index plot of $1/B_n$ vs. n fits a straight line that intercepts the n-axis at γ = -0.45±0.02, again consistent with a Dirac spectrum.

The expanded plot shows why intense fields are needed to fix γ reliably. By accessing the $n = \frac{1}{2}$ index at 45 T (Figs. 4c,d), we have reduced considerably the "spread" of intercepts caused by the measurement uncertainties: an intercept γ = 0 may be safely excluded. A more subtle point is the slight curvature of the index plot. In Fig. 4c, if we extrapolate the best-fit line (dashed) using the total data set from 3 to 45 T, its intercept yields -0.78, nearly exactly between -1 and -$\frac{1}{2}$. By contrast, the best-fit line (bold) to the high-field extrema for $n \leq 3$ yields an intercept (-0.61) closer to -$\frac{1}{2}$. This implies that the index curve $1/B_n$ vs. n develops a slight curvature in intense fields. (The curvature accounts for the low-B phase shift apparent in the single-frequency fit in Fig. 3a.)

A possible cause of curvature is the spin-Zeeman energy. When that is included, the Hamiltonian is

$$H = v_F \hat{\mathbf{n}} \cdot \boldsymbol{\sigma} \times \boldsymbol{\pi} - \frac{g\mu_B}{2}\mathbf{B} \cdot \boldsymbol{\sigma} \quad (2)$$

where $\hat{\mathbf{n}}$ the unit vector normal to the surface. $\boldsymbol{\sigma}$ are the spin Pauli matrices, and $\boldsymbol{\pi} = \mathbf{p} - e\mathbf{A}$ is the momentum $\mathbf{p}$ of the electron in a vector potential $\mathbf{A}$. The LL energy is given by

$$E_n = \pm\sqrt{2n\hbar v_F^2 eB + (g\mu_B B/2)^2}. \quad (3)$$

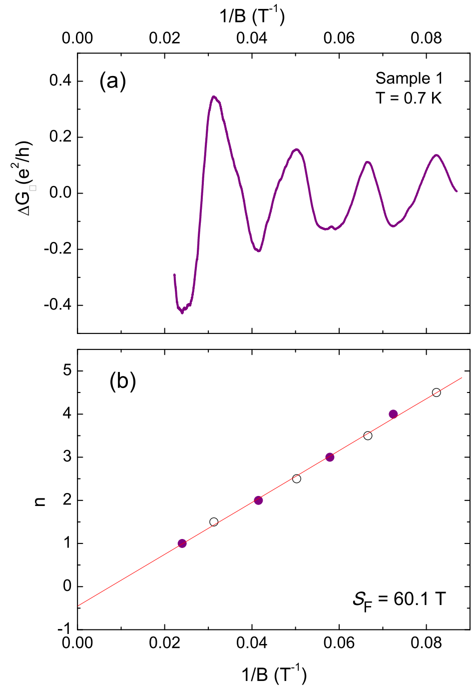

FIG. 5: (color online) The oscillatory component ΔG_{xx} vs. $1/B$ (Panel a) and the index plot of $1/B_n$ vs. n (Panel b) in Sample 1. The intercept γ of the best-fit line is -0.45±0.02.

The energy of the $n = 0$ LL increases linearly with B instead of being unshifted. For a large g, the plot of $1/B_n$ vs. n will deviate from a straight line as $1/B \to 0$. In our experiment, we have tracked the LLs to n = 1. The weak deviation from a straight line in Fig. 4c) is inconsistent with values of g substantially larger than 2. More importantly, however, the observed deviation is opposite in sign to that predicted by Eq. 3. As we do not see evidence for a deviation caused by a large g-factor, we conclude that the the g factor of the surface states in Bi_2Te_2Se are not significantly greater than 2 in the quantum limit.

V. SURFACE CARRIER MOBILITY

In general, it is very difficult to separate G^s from G^b reliably even at $B = 0$. Shubnikov de-Haas (SdH) oscillations – when measured with sufficient resolution – provide a powerful way to tease out the surface conductance. Analysis of the SdH amplitude vs. B yields the scattering rate and the surface mobility μ_s (equivalently the mean-free-path ℓ). Also, the period of the oscillations yields k_F. With μ_s and k_F known, we then obtain the zero-B value of $G^s_{xx} \equiv G^s$ using

$$G^s = (e^2/h)k_F\ell. \quad (4)$$

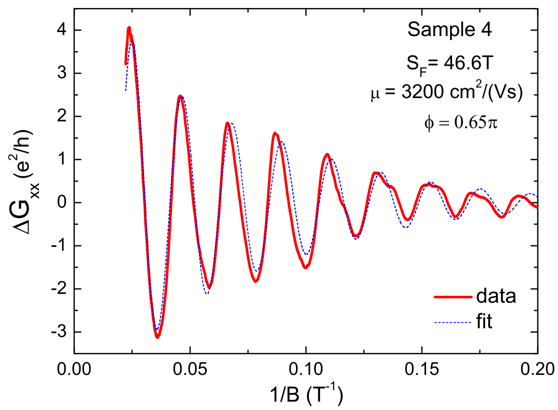

FIG. 6: (Color online) The oscillatory component of the conductance ΔG_{xx} in Sample 4 at 0.7 K (solid curve) and the fit to Eq. 5 using only one frequency (dashed curve).

To focus on the SdH oscillations, we first determine the envelope curves passing through the extrema of the oscillations as explained in Fig. 2 of the main text. The oscillatory component ΔG_{xx} is obtained by subtracting from G_{xx} the background, defined as the curve lying between the envelope curves. (We remark that ΔG_{xx} does not account for all of the surface conductance. By construction, its field-averaged value $\langle \Delta G_{xx} \rangle_B$ vanishes. Hence we must have $\Delta G_{xx} < G^s_{xx}$.)

To fit the oscillatory component ΔG_{xx}, we employed the standard Lifshitz-Kosevich expression[24]

$$\frac{\Delta G_{xx}}{G_{xx}} = \left(\frac{\hbar\omega_c}{2E_F}\right)^{\frac{1}{2}} \frac{\lambda}{\sinh\lambda} e^{-\lambda_D} \cos\left[\frac{2\pi E_F}{\hbar\omega_c} + \varphi\right], \quad (5)$$

with $\lambda = 2\pi^2 k_B T/\hbar\omega_c$ and $\lambda_D = 2\pi^2 k_B T_D/\hbar\omega_c$, where ω_c is the cyclotron frequency and the Dingle temperature is given by $T_D = \hbar/(2\pi k_B \tau)$, with τ the lifetime. For 2D systems, we may write the SdH frequency as $2\pi E_F B/(\hbar\omega_c)$, which simplifies to $4\pi^2\hbar n_s/e$, with the 2D carrier density $n_s = k_F^2/4\pi$ (per spin). Equation 5 may be employed in a Dirac system if we write the cyclotron mass as $m_c = E/v_F^2$.

As shown in Fig. 6, we obtain a reasonably close fit to the observed oscillations (bold curve) using just one frequency. The optimal fit yields for the 3 adjustable parameters the values $k_F = 0.038$ Å^{-1}, $\varphi = 0.65\pi$ and $T_D = 8.5\pm1.5$ K, which implies a surface mean-free-path $\ell = 79\pm8$ nm and mobility $\mu_s = e\ell/\hbar k_F = 3{,}200\pm300$ cm^2/Vs. The metallicity parameter $k_F\ell$ equals 30. We estimate that, in Sample 4 at B=0, G^s accounts for ∼ 19% of the total observed conductance. These values are similar to those obtained in an earlier sample, which had a slightly larger k_F (0.047 Å^{-1})[19].

The mobility provides a strong, quantitative argument that the SdH oscillations arise from surface states. Suppose for the sake of argument that the oscillations arise from bulk states. The SdH period is then to be identified with a 3D Fermi sphere of radius $k_F = 0.038$ Å^{-1}, or a 3D carrier density of 1.86×10^{18} cm^{-3}. With this density, the inferred mobility gives a 3D resistivity $\rho_b \sim$ 1.1 mΩcm at 4 K. Instead we measure ρ to be 5 Ωcm. The large discrepancy (factor of 4,500) firmly precludes a bulk origin for the SdH oscillations.

VI. CONCLUSIONS

The Dirac-like topological surface states detected in ARPES and STM experiments present a host of new opportunities for transport experiments especially in high magnetic fields. In bulk crystals, the presence of bulk carriers complicate transport studies. As shown here, quantum oscillations provide a powerful way to isolate the surface carriers and to determine their mobility and $k_F\ell$. The index plot of the integers n versus $1/B_n$ can be used to confirm the π-shift associated with the Berry phase of the surface electrons, which leads to an intercept -$\frac{1}{2}$ in the limit $1/B \to 0$. To access LLs at $n = 1$ (or lower), we have employed fields up to 45 T. The results in Figs. 4 and 5 provide direct confirmation of the existence of the -$\frac{1}{2}$ intercept expected from a Dirac disperion.

The resolution attained here provides experimental verification of the point that the -$\frac{1}{2}$ intercept is observed only when B_n is identified with minima in G_{xx} or maxima in R_{xx}. (For contrast, we note a recent report[25] in which a -$\frac{1}{2}$ intercept was obtained in high-B measurements on exfoliated crystals of Bi_2Te_3. However, because B_n was inferred from minima in the resistivity, it seems that the -$\frac{1}{2}$ intercept actually implies a Berry phase that is zero, consistent with SdH oscillations from conventional bulk carriers.)

The linearity of the index plot in Figs. 4 and 5 show that the Lande g-factor is small (g ∼2). The $n = 0$ LL is unshifted even at 45 T, consistent with STM experiments taken at 11 T[10,11].

Finally, we comment on the results in the large-B limit. In Fig. 3a, the last maximum in ΔG_{xx} (at $B \simeq 40$ T) corresponds to $n = \frac{1}{2}$ (see arrow in the index plot in Fig. 4c). At this field, the Fermi energy E_F is aligned with the center of the $n = 1$ LL, as sketched in the inset in Fig. 4c. In our indexing scheme, there is 1 filled LL between E_F and the Dirac Point, with $\frac{1}{2}$ of the filled states from the unshifted LL at the Dirac Point). Hence, these results provide rather firm evidence for this $\frac{1}{2}$-shift in the limit $1/B \to 0$. As the inset in Fig. 4c implies, the interesting states in the $n = 0$ LL in Sample 4 become experimentally accessible in fields higher than 45 T.

We acknowledge valuable discussions with Liang Fu, Xiao Liang Qi and Joel Moore. The research is supported by the US National Science Foundation (grant DMR 0819860) and the Army Research Office (ARO W911NF-11-1-0379). Sample growth and characterization were supported by an award from the Defense

Advanced Research Projects Agency under SPAWAR Grant No.: N66001-11-1-4110. The experiments were performed at the National High Magnetic Field Laboratory, which is supported by NSF Cooperative Agreement No. DMR-084173, by the State of Florida, and by the Department of Energy. YKL acknowledges support from the China Scholarship Council (CSC).

* *Current address of YKL*: Department of Physics, Zhejiang University, Hangzhou, China.

[1] L. Fu, C. L. Kane, E. J. Mele, Phys. Rev. Lett. **98**, 106803 (2007).

[2] L. Fu, C. L. Kane, Phys. Rev. B **76**, 045302 (2007).

[3] J. E. Moore, L. Balents, Phys. Rev. B **75**, 121306(R) (2007).

[4] B. A. Bernevig, T. Hughes, S. C. Zhang, Science **314**, 1757-1761 (2006).

[5] D. Hsieh, D. Qian, L. Wray, Y. Xia, Y. S. Hor, R. J. Cava and M. Z. Hasan Nature **452**, 970-974 (2008).

[6] D. Hsieh, Y. Xia, L. Wray, D. Qian, A. Pal, J. H. Dil, J. Osterwalder, F. Meier, G. Bihlmayer, C. L. Kane, Y. S. Hor, R. J. Cava, and M. Z. Hasan, Science **323**, 919-922 (2009).

[7] Y. Xia, D. Qian, D. Hsieh, L. Wray, A. Pal, H. Lin, A. Bansil, D. Grauer, Y. S. Hor, R. J. Cava and M. Z. Hasan, Nature Phys **5**, 398-402 (2009).

[8] Y. L. Chen, J. G. Analytis, J.-H. Chu, Z. K. Liu, S.-K. Mo, X. L. Qi, H. J. Zhang, D. H. Lu, X. Dai, Z. Fang, S. C. Zhang, I. R. Fisher, Z. Hussain, and Z.-X. Shen, Science **325**, 178-181 (2009).

[9] P. Roushan, Jungpil Seo, Colin V. Parker, Y. S. Hor, D. Hsieh, Dong Qian, Anthony Richardella, M. Z. Hasan, R. J. Cava, Ali Yazdani, Nature **460**, 1106 (2009).

[10] T. Hanaguri, K. Igarashi, M. Kawamura, H. Takagi, and T. Sasagawa, Phys. Rev. B **82**, 081305(R) (2010).

[11] Peng Cheng *et al.*, Phys. Rev. Lett. **105**, 076801 (2010).

[12] Dong-Xia Qu, Y. S. Hor, Jun Xiong, R. J. Cava and N. P. Ong, Science **329**, 821 (2010).

[13] James G. Analytis, Ross D. McDonald, Scott C. Riggs, Jiun-Haw Chu, G. S. Boebinger and Ian R. Fisher, Nature Physics **6**, 960 (2010).

[14] C. Brüne, C. X. Liu, E. G. Novik, E. M. Hankiewicz, H. Buhmann, Y. L. Chen, X. L. Qi, Z. X. Shen, S. C. Zhang, and L. W. Molenkamp, Phys. Rev. Lett. **106**, 126803 (2011).

[15] Yuanbo Zhang, Yan-Wen Tan, Horst L. Stormer and Philip Kim, Nature **438**, 201 (2005).

[16] We are indebted to Liang Fu for clarifying this point.

[17] A. A. Taskin and Yoichi Ando, Phys. Rev. B **84**, 035301 (2011).

[18] Zhi Ren, A. A. Taskin, Satoshi Sasaki, Kouji Segawa, and Yoichi Ando, Phys. Rev. B **82**, 241306(R) (2010).

[19] Jun Xiong, A.C. Petersen, Dongxia Qu, Y.S. Hor, R.J. Cava, N.P. Ong, Physica E **44**, 917 (2012).

[20] S. Jia, H. W. Ji, E. Climent-Pascual, M. K. Fuccillo, M. E. Charles, J. Xiong, N. P. Ong, and R. J. Cava, Phys. Rev. B **84** 235206 (2011).

[21] Yongkang Luo, Stephen Rowley, Jun Xiong, Shuang Jia, R. J. Cava, N. P. Ong, arXiv:1110.1081v1.

[22] Su-Yang Xu, L. A. Wray, Y. Xia, R. Shankar, A. Petersen, A. Fedorov, H. Lin, A. Bansil, Y. S. Hor, D. Grauer, R. J. Cava, M. Z. Hasan, arXiv:1007.5111v1.

[23] H. H. Sample, W. J. Bruno, S. B. Sample, and E. K. Sichel, Jnl. Appl. Phys. **61**, 1079 (1987).

[24] L. M. Roth and P. N. Argyres, in Semiconductors and Semimetals, edited by R. K. Williardson and A. C. Beer (Academic Press, New York, 1966), Vol. 1.

[25] M. Veldhorst, M. Snelder, M. Hoek, T. Gang, X.L. Wang, V.K. Guduru, U. Zeitler, W.G. v.d. Wiel, A.A. Golubov, H. Hilgenkamp, and A. Brinkman, Nature Materials **11**, 417 (2012).